0026-895X/95/010001-09$03.00/0

MOLECULAR PHARMACOLOGY, 47:1-9, 1995

Site-Selective Photoaffinity Labeling of the *Torpedo californica* Nicotinic Acetylcholine Receptor by Azide Derivatives of Ethidium Bromide

STEEN E. PEDERSEN

Department of Molecular Physiology and Biophysics, Baylor College of Medicine, Houston, Texas 77030

Received August 19, 1994; Accepted October 19, 1994

SUMMARY

Three azido derivatives of ethidium bromide, a potent noncompetitive antagonist of the nicotinic acetylcholine receptor from *Torpedo californica*, were synthesized, namely 8-azido-ethidium chloride, 3-azido-ethidium chloride, and 3,8-diazido-ethidium chloride. These derivatives were tested for their ability to interact with the noncompetitive antagonist binding site and the acetylcholine binding sites on the acetylcholine receptor. The derivatives bound to the noncompetitive antagonist site with 2–5-fold lower affinity than did ethidium bromide, as determined by competitive inhibition of [^{3}H]phencyclidine binding, indicating a moderate effect of the azide groups upon binding. Inhibition of [^{3}H]-acetylcholine binding by ethidium and its azide derivatives indicated differential binding to the two agonist sites, with high affinity binding to the same site that exhibits high affinity for *d*-tubocurarine. Photoaffinity labeling by these derivatives revealed reaction with the α and γ subunits that was specific for the acetylcholine binding sites. Inhibition of labeling by *d*-tubocurarine showed reaction with α subunits at both of the acetylcholine binding sites, whereas reaction with the γ subunit was consistent with reaction only at the site with high affinity for *d*-tubocurarine. There was no corresponding reaction with the δ subunit, which forms part of the second acetylcholine binding site, despite reaction with the apposing α subunit. The azides, therefore, display preferential reaction with the γ subunit. The selectivity of the reaction must reflect structural differences between the two sites, and subsequent determination of the labeled site(s) should reveal the nature of the differences.

The nicotinic AChR from *Torpedo californica* electric organ is a ligand-gated cation channel composed of homologous subunits, with a stoichiometry of $\alpha_2\beta\gamma\delta$ (1, 2). The five subunits each traverse the lipid bilayer and form a pseudosymmetric pentameric rosette with the channel located at the central axis (3). Channel opening is regulated by the binding of two molecules of ACh to sites on the extracellular surface of the protein (see Ref. 4 for review).

Affinity labeling of ACh binding sites using sulfhydryl-reactive compounds initially identified the α subunit as the site of ACh binding (5, 6). The snake venom toxin α-bungarotoxin could also be shown to bind with moderate affinity to the α subunit, even when denatured and proteolyzed (7). Further studies using affinity labeling followed by mapping of the labeled sites to the amino acid sequence have identified residues in the α subunit involved in ACh binding, i.e., Cys-192 and -193 (8) and the nearby residues Tyr-190 (9, 10) and Tyr-198 (11), as well as residues more distant in the sequence, Trp-149 (10) and Tyr-93 (12). The region α186 to α211 also binds α-bungarotoxin with low affinity, and the residues identified by affinity labeling contribute substantially to this binding, as judged by mutagenesis of these residues (13).

The ACh binding sites are nonidentical and can be distinguished by the differential binding of the plant alkaloid *d*-tubocurarine (14). A combination of α and γ subunits comprise the site that binds *d*-tubocurarine with high affinity, whereas the second α subunit and the δ subunit comprise the site that has low affinity for *d*-tubocurarine (15, 16), and the distinct affinities of the two sites must arise from the differing contributions of the γ and δ subunits. Affinity labeling of the *Torpedo* receptor with *d*-[^{3}H]tubocurarine has identified γTrp-56 and δTrp-57 as labeled residues (17). Because this residue is conserved between the γ and δ subunits, it is unlikely to contribute to the distinct affinities. Site-directed mutagenesis of three residues of the mouse muscle AChR γ subunit (γIle-116, γTyr-117, and γSer-161) to the corresponding residues of

This work was supported by grants from the Muscular Dystrophy Association and the National Institutes of Health (NS28879). S.E.P. is the recipient of Research Career Development Award NS01618.

ABBREVIATIONS: AChR, acetylcholine receptor; ACh, acetylcholine; EB, ethidium bromide (3,8-diamino-5-ethyl-6-phenylphenanthridinium bromide); 3-AEB, 3-azido-8-amino-5-ethyl-6-phenylphenanthridinium chloride; 8-AEB, 3-amino-8-azido-5-ethyl-6-phenylphenanthridinium chloride; di-AEB, 3,8-diazido-5-ethyl-6-phenylphenanthridinium chloride; TFA, trifluoroacetic acid; NCA, noncompetitive antagonist; HEPES, 4-(2-hydroxyethyl)-1-piperazineethanesulfonic acid; HTPS, HEPES-*Torpedo* physiological saline; PCP, phencyclidine; SDS, sodium dodecyl sulfate; PAGE, polyacrylamide gel electrophoresis; HPLC, high pressure liquid chromatography; DTT, dithiothreitol.

the δ subunit could completely change the affinity to that characteristic of the α and δ subunit combination (18).

The interactions of EB with the AChR were first described as competitive antagonism (19–21), with concomitant enhancement of fluorescence. Work by Herz *et al.* (22) demonstrated that binding to the NCA site resulted in fluorescence enhancement. Binding of EB to the NCA site is highly dependent on the conformational state of the receptor and requires the presence of a desensitizing ligand at the ACh binding sites, whereas affinity is reduced markedly in the presence of α-bungarotoxin, which does not stabilize the desensitized state. Binding of EB to the ACh binding sites was also demonstrated by Herz *et al.* (22), but with lower affinity than binding to the NCA site.

Azido derivatives of EB have been synthesized and characterized with respect to their binding and reaction with DNA (23, 24). In this article we describe the reaction of three azide derivatives of EB (8-AEB, 3-AEB, and di-AEB) with the AChR and show that the photoaffinity reactions of the derivatives with the AChR were qualitatively similar but differed in the extent of reaction, as detected by fluorescence intensity. Surprisingly, little formation of fluorescent adducts was detected at the NCA site, whereas there was clear reaction at the ACh binding sites. There was reaction with the α subunits at both ACh binding sites. There was also reaction with the γ subunit at the high affinity site but not with the corresponding δ subunit at the second site. Thus, we show that these compounds are selective in their reactivity, a novel feature that must reflect differences among the sites that may also account for the site selectivity towards some antagonists.

Experimental Procedures

Materials. AChR-rich membranes were isolated from *T. californica* electric organ (Marinus Inc., Long Beach, CA) as described in Pedersen *et al.* (25), with the addition of calpain inhibitors I and II (10 mg/kg of organ). Purified membranes typically contained 1.4 nmol of ACh binding sites/mg of protein, measured by binding of [^{3}H]ACh as described below (26). Membranes were stored in 37% sucrose/0.02% NaN_3 at −80° under argon. Lower specific activity fractions (35% sucrose; 0.2–0.5 nmol of ACh binding sites/mg of protein) were sometimes used for binding assays. EB, lauryl sulfate, 2-mercaptoethanol, *N,N,N′,N′*-tetramethylethylenediamine, tetracaine, α-bungarotoxin, carbamylcholine, and Tris were from Sigma Chemical Co.; SDS and TFA were from Pierce; diisopropylfluorophosphate was from Aldrich. Proadifen hydrochloride was obtained from Research Biochemicals, and meproadifen iodide was synthesized by methylation of the free base of proadifen, as described by Krodel *et al.* (26), and was crystallized from ethanol. Acrylamide, bisacrylamide, and HEPES were from Boehringer Mannheim. Most reactions and assays were carried out in HTPS (250 mM NaCl, 5 mM KCl, 3 mM $CaCl_2$, 2 mM $MgCl_2$, 0.02% NaN_3, 20 mM HEPES, pH 7.0). NaN_3 was omitted for photoreactions and spectroscopy. [^{3}H]ACh (74 Ci/mol) was obtained from Amersham, [^{3}H]PCP (52 Ci/mmol) was obtained from New England Nuclear, and *d*-[^{3}H]-tubocurarine (11 Ci/mmol) was kindly donated by David C. Chiara and Jonathan B. Cohen (Department of Neurobiology, Harvard University).

Synthesis of azide derivatives of EB. Three azido derivatives of EB (I) (Fig. 1), i.e., 3-AEB (II), 8-AEB (III), and di-AEB (IV), were synthesized essentially according to the method of Firth *et al.* (23), with the modifications described below. The reactions and purity of the compounds were routinely monitored by reverse phase HPLC, which permitted rapid separation and quantitation of each of the four species encountered (Fig. 2). HPLC was performed using a Beckman Ultraspherogel C_{18}, 5-μm, 4.6- × 250-mm column eluted with a gradient of increasing acetonitrile containing TFA (0.1%).

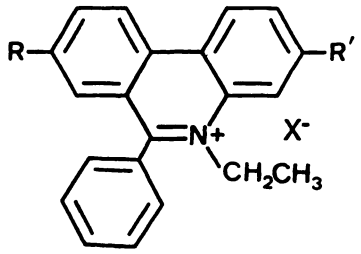

R	R'	X⁻	
NH_2	NH_2	Br^-	Ethidium Bromide
NH_2	N_3	Cl^-	3-Azido Ethidium Chloride
N_3	NH_2	Cl^-	8-Azido Ethidium Chloride
N_3	N_3	Cl^-	di-Azido Ethidium Chloride

Fig. 1. Structures of EB and azido derivatives.

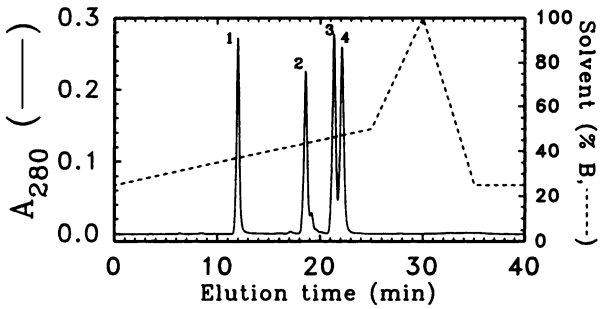

Fig. 2. HPLC elution of EB and azido derivatives. A mixture of EB, 3-AEB, 8-AEB, and di-AEB (25 pmol each, ~1 μg) was injected onto a C_{18} reverse phase column and eluted with a gradient of solvent B (– – –). Elution was monitored by absorbance at 280 nm (——). *Peak 1*, EB; *peak 2*, 3-AEB; *peak 3*, 8-AEB; *peak 4*, di-AEB. Solvent A was water/0.1% TFA, and solvent B was acetonitrile/0.09% TFA.

For di-AEB synthesis, 0.57 g of EB (1.4 mmol) dissolved in water was cooled on ice and reacted with 14 mmol of $NaNO_2$ for 10 min in 0.1 M HCl, followed by addition of NaN_3 (14 mmol) dissolved in water. The product was precipitated with base, filtered, and dried (72% yield). Purity was 89%, as judged by reverse phase HPLC (Fig. 2). For synthesis of 8-AEB, 0.50 g of EB (1.3 mmol) was reacted with 1 equivalent of $NaNO_2$ for 3 min at 0°, followed by addition of 1.5 mmol of NaN_3, which was allowed to react overnight. This yielded a mixture of all four compounds, with 8-AEB being predominant. 8-AEB was purified by chromatography on a CM-Sephadex column (1.0 × 20 cm; Pharmacia) and eluted with HCl as described by Firth *et al.* (23). The final yield was 14% and the purity was 85%, as judged by HPLC. For synthesis of 3-AEB, EB (1 g, 2.5 mmol) was first reacted with two additions of acetic anhydride (2.5 mmol each), in water, to block the more reactive 8-amino group. The product, 8-acetamido-EB, was collected by filtration, resuspended, heated to 60° for 1 hr to dissolve unreacted EB, cooled, and then recollected by filtration. 8-Acetamido-EB (0.595 g, 1.4 mmol) was then reacted with 9 mmol of $NaNO_2$ for 10 min in 0.1 N HCl, followed by reaction with 9 mmol of NaN_3 for 3 hr at 0°. The acetamido moiety was converted to the amine by heating of the precipitated product at 70° for 2 hr in 2 N HCl. The 3-AEB was then purified by cation exchange chromatography; the products were eluted from the column with a gradient of NaCl, rather than a gradient of HCl, resulting in elution in a smaller volume. The fractions containing 3-AEB were made basic by addition of 5 N NaOH, and the carbinol base was extracted into methylene chloride. This was dried and stored (26% yield). 3-AEB was 98% pure, as judged by reverse phase HPLC.

Each compound was unambiguously identified by UV/visible absorption spectroscopy, which yielded maxima identical to those reported by Firth *et al.* (23), and by electrospray mass spectroscopy. Each mass spectrum yielded peaks that corresponded to the predicted masses of the positive ions and a smaller peak or peaks due to *in situ* photolysis of the azide to form the nitrene. Mass spectroscopy was carried out at

the Baylor Core Mass Spectroscopy Facility. Purity of the compounds was judged chromatographically by HPLC (Fig. 2) and by comparison of absorption spectra with the data of Firth *et al.* (23). The presence of the azide was confirmed by sensitivity of the compounds to both visible and UV irradiation, as observed by changes in fluorescence and disappearance of the compounds from HPLC traces, and, for di-AEB, by IR spectra.

Photoreaction methods. Samples of AChR were routinely irradiated in the presence of the azide derivatives of EB in microtiter plates. Usually 50 μg of AChR-rich membranes in 200 μl of HTPS were irradiated for 2 min with a 15-W light bulb through a Plexiglas shield or irradiated directly with a UV lamp (Spectroline EF-160C, at 254 nm) for 20 sec to 1 min. The two methods produced similar specific reactions, but irradiation with the UV lamp resulted in more nonspecific reaction. The photoreactions were terminated by addition of DTT to 50 mM and carbamylcholine to 5 mM, to destroy the azide and block binding to the ACh binding sites, respectively. The samples were centrifuged (19,000 × *g* for 30 min) to collect the membranes, which were then dissolved in sample buffer for gel electrophoresis. SDS-PAGE to separate the subunits of the AChR was carried out essentially according to the method of Laemmli (27) as described by Pedersen *et al.* (25), using separating gels with a 7.5% concentration of polyacrylamide and a 25:1 ratio of acrylamide to bisacrylamide. Fluorescence was visualized on a UV transilluminator and photographed through an orange filter. The treatment of the reaction mixtures with DTT and carbamylcholine after photoreaction effectively blocked some nonspecific labeling that ocurred during the sample workup, likely due to reaction of the azides with free sulfhydryl groups after dissolution in sample buffer, and blocked some light-independent and apparently specific labeling that was likely due to reaction after centrifugation of the reaction mixture.

Densitometry. Film negatives (Polaroid type 55 film) were analyzed by two-dimensional laser densitometry, using an LKB 2222 UltroScan XL laser densitometer, to quantitate the relative fluorescence of labeled α and γ subunits. The absorbance was recorded in 0.28-mm pixels across both dimensions of the film. Rescanning of the film resulted in reproducible pixel intensities. The data were transferred to a computer and stored in a spreadsheet (Microsoft Excel 4.0). Volume integration of fluorescence in α and γ subunit bands was performed by summing the absorbance values for the pixels in a rectangular area including the band. Background absorbance values were averaged from pixel lines immediately above and below each band and were subtracted from the value for each pixel in the integrated area. This eliminated substantial error due to variation in background across the film. Exposures were limited to keep the absorbance in a range of approximately linear intensity. This limit was determined by loading varying amounts of labeled AChR-rich membranes, mixed with a compensating amount of unlabeled membranes to keep the protein load constant, and examining the relationship between load, integrated volume, and exposure time. This volume integration technique displayed slight curvature in relation to the amount of fluorescent AChR loaded onto the gel and is thus not perfectly quantitative. Therefore, exposures of two different times were routinely taken for each gel for densitometric analysis. In the instances where both exposures were analyzed, the integrated results were similar. In several experiments the data were separately analyzed by two persons and also yielded similar results.

Ligand binding assays. Ligand binding assays with [^{3}H]ACh (74 Ci/mol), [^{3}H]PCP (52 Ci/mmol), or *d*-[^{3}H]tubocurarine (0.25 Ci/mmol, isotopically diluted from a 11 Ci/mmol stock solution) were performed by centrifugation, according to the procedure of Krodel *et al.* (26). AChR-rich membranes or a less pure side fraction of membranes from the discontinuous sucrose gradient fractionation (50 μg) were incubated in HTPS at room temperature, with the indicated concentrations of ligand, for 30 min in the dark. For [^{3}H]ACh binding assays, the membranes were first incubated with diisopropylfluorophosphonate (26) to inactivate acetylcholinesterase. The membranes were centrifuged at 19,000 × *g* for 30 min in a TOMY MTX-150 microcentrifuge, to separate bound from free ligand. The free ligand concentration was determined by counting an aliquot of the supernatant. Bound ligand was determined by counting the pellet after dissolution in 10% SDS. Nonspecific binding was determined by inclusion of a competitive inhibitor at high concentration. Inhibition data were analyzed by nonlinear least-squares fitting of the data to models for single-site inhibition, $B = A/(1 + I/K_{app}) + Nsp$, and for two-site inhibition, $B = A[1/(1 + I/K_{app1}) + 1/(1 + I/K_{app2})] + Nsp$, where B is the concentration bound, A is the maximum concentration bound, Nsp is the nonspecific binding, and K_{app} is the concentration of inhibitor required to reduce the concentration of specifically bound ligand by 50%. Fitting was done using the program SigmaPlot (version 4.1; Jandel Scientific). Equilibrium dissociation constants (K_i) were determined from the K_{app} values using the equation $K_i = K_{app} \cdot K_d/(K_d + L)$, where L is the free radioactive ligand concentration and K_d is the equilibrium dissociation constant for the radioactive ligand. The K_d values for [^{3}H]ACh and *d*-[^{3}H]tubocuarine were determined in independent experiments to be 20 nM and 50 nM (for the high affinity site), respectively.

Ancillary methods. Fluorescence spectra were collected with an SLM-8000 fluorescence spectrophotometer, using a cooled photomultiplier biased for photon counting. To collect emission spectra of labeled subunits, EB, and photolyzed azide derivatives, samples were excited at 500 nm (with a 16-nm bandwidth) and fluorescence was collected using a 4-nm bandwidth. Both excitation light and emission light were filtered with 470-nm cut-off filters. Emission spectra were independent of the excitation wavelength; similar spectra were obtained by excitation at 280 nm. The emission spectra were not corrected: the dips at 630 nm in the emission spectra are a fluorometer artifact, due to the Woods grating anomaly, and are not a property of the fluorescence spectra.

Protein assays were performed using a bicinchoninic acid microassay (Pierce), with bovine serum albumin as a standard. HPLC was performed using a Beckman 125 pump; detection was by absorbance, using a Beckman 166 variable wavelength detector, and gradient formation and data collection were computer controlled using Beckman System Gold software. Labeled subunits were isolated by passive elution from excised gel slices using the procedure of Hager and Burgess (28), as described by Pedersen *et al.* (29).

Results

Photoaffinity labeling. EB is a potent NCA of the AChR that binds to a site within the ion channel (30, 31). Three azido derivatives of EB were synthesized as described in Experimental Procedures (Fig. 1), for use as photoaffinity labels that might ultimately lead to the identification of amino acids involved in ligand binding at the NCA site.

Irradiation of a mixture of 3-AEB and AChR-rich membranes with either UV or visible light resulted in reaction with the AChR (Fig. 3). Adducts were visualized on a UV light-box after separation of AChR subunits by SDS-PAGE. Fluorescence was observed indicating reaction with the α subunit, a band migrating above the 43-kDa protein, and the γ subunit and, to a lesser extent, a band of 90 kDa, the 43-kDa protein, the β subunit, and the δ subunit (Fig. 3, *lane 2*). The pharmacological specificity of the reaction with 3-AEB was examined by the inclusion of competitive ligands for both the ACh binding sites and the NCA site. Inclusion of the agonist carbamylcholine (Fig. 3, *lane 3*) reduced the fluorescence associated with the α and γ subunits and the band migrating above the 43-kDa protein, whereas the fluorescence of the remaining bands was unaffected. The labeling was similarly inhibited by the competitive antagonists *d*-tubocurarine (Fig. 3, *lane 4*) and α-bungarotoxin (Fig. 3, *lane 5*), which also bind to the ACh binding sites. In contrast, the NCAs PCP (Fig. 3, *lane 6*),

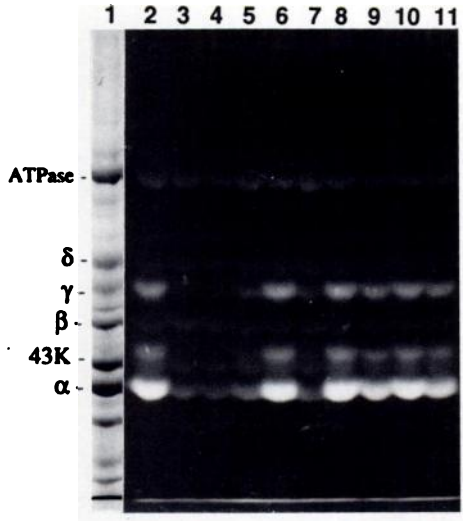

Fig. 3. Pharmacological specificity of reaction of 3-AEB with the AChR. AChR-rich membranes (50 μg) were reacted with 10 μM 3-AEB by irradiation with visible light, as described in Experimental Procedures, in the presence of the following: no additions (*lanes 2* and *10*), 1 mM carbamylcholine (*lane 3*), 50 μM *d*-tubocurarine (*lane 4*), 2 μM α-bungarotoxin (*lane 5*), 30 μM PCP (*lane 6*), 30 μM PCP plus 1 mM carbamylcholine (*lane 7*), 50 μM proadifen (*lane 8*), 30 μM tetracaine (*lane 9*), or 50 μM meproadifen (*lane 11*). Subunits were separated by SDS-PAGE and fluorescence was visualized on a UV transilluminator. *Lane 1*, Coomassie blue-stained lane of the same gel. The migration of the individual AChR subunits and the α subunit of Na^+/K^+-ATPase is indicated on the *left*.

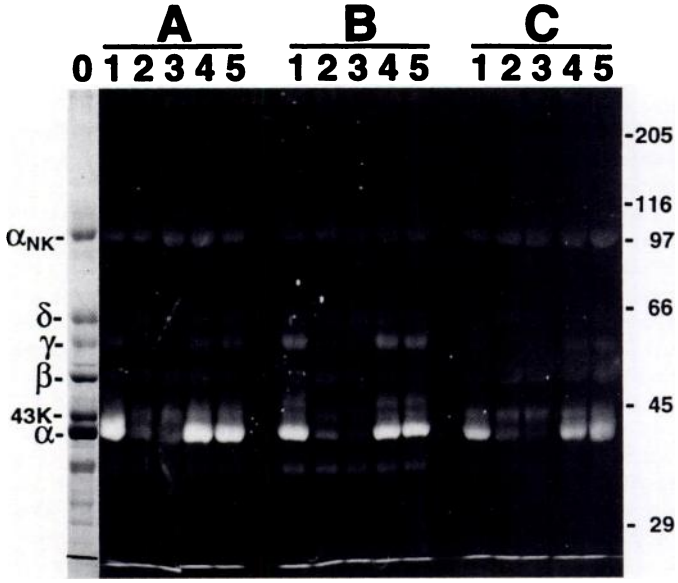

Fig. 4. Photoaffinity labeling of the AChR by the three azido derivatives of EB. AChR-rich membranes (50 μg in 200 μl) were reacted with 5 μM 8-AEB (A), 3-AEB (B), or di-AEB (C) by UV irradiation, as described in Experimental Procedures. Reactions contained the following reagents: no additions (*lanes 1* and *5*), 1 mM carbamylcholine (*lanes 2*), 1 mM carbamylcholine plus 100 μM PCP (*lanes 3*), or 100 μM PCP (*lanes 4*). *Lane 0*, Coomassie blue-stained lane of the gel. The migration of the individual AChR subunits and the α subunit of Na^+/K^+-ATPase (α_{NK}) is indicated on the *left* and that of the molecular weight standards is indicated on the *right* (myosin, 205,000; β-galactosidase, 116,000; phosphorylase B, 97,400; bovine serum albumin, 66,000; ovalbumin, 45,000; carbonic anhydrase, 29,000).

proadifen (Fig. 3, *lane 8*), tetracaine (Fig. 3, *lane 9*), and meproadifen (Fig. 3, *lane 11*) had little or no effect on the fluorescence labeling. Inhibition by three competitive ligands for the ACh binding sites is consistent with reaction of 3-AEB at this site, whereas lack of inhibition by four NCAs demonstrates that a fluorescent adduct is not formed at the NCA site. The reaction at the γ subunit parallels that at the α subunit, suggesting that affinity labeling reflects binding to the same site. The band migrating above the 43-kDa protein is an α subunit that migrates anomalously and is an artifact of irradiation (15).

The azido derivatives 8-AEB (Fig. 4A), 3-AEB (Fig. 4B), and di-AEB (Fig. 4C) were compared for reactivity with the AChR. In the presence of the agonist carbamylcholine, reaction at the α subunit was diminished for all three compounds (Fig. 4, compare *lanes 1* and *2*), whereas the presence of the NCA PCP alone had little or no effect (Fig. 4, *lanes 4*). In addition to the labeling of the α subunit, labeling of the γ subunit could also be blocked by carbamylcholine, but the extent of reaction was variable for the three azides. Reaction with the γ subunit was strongest for 3-AEB, weaker for 8-AEB, and nearly undetectable for di-AEB. Inhibition of labeling by carbamylcholine and failure of PCP to affect labeling suggested that the sites of labeling by all three azide derivatives were at one or both ACh binding sites. Nonetheless, for 3-AEB and di-AEB, addition of PCP in the presence of carbamylcholine (Fig. 4, B and C, *lanes 3*) decreased the remaining fluorescence in the α subunit, suggesting that a minor fraction of the fluorescence may be due to reaction at the NCA site.

Inclusion of oxidized glutathione or 2-mercaptoethanol as scavengers (15) in the photoreactions had little effect on specific labeling but could decrease nonspecific reaction at concentrations greater than 1 mM (data not shown). The effect was not pronounced and these compounds were not used routinely, but the lack of effect on specific labeling suggests that the photoreaction is not due to long-lived activated species or reaction at a distant site on the protein after diffusion of the active species away from the binding site. Specific labeling could be induced using either UV irradiation or visible irradiation with the UV component blocked. This demonstrated that the irradiation activated the ligand rather than amino acids within the binding site, because the ligand absorbs visible light and the protein does not.

Binding properties of EB and the azido derivatives. The apparent lack of reaction of the azido compounds at the NCA site may be attributable to one or more of the following factors: the azido derivatives may have markedly lower affinity for the NCA site, compared with EB, and the lack of reaction may simply reflect lack of binding to the NCA site; they may bind to the NCA site and fail to react after photoexcitation; or they may react and yield nonfluorescent adducts at the NCA site that were not detected. To examine the first possiblity, the affinities of EB and its three azido derivatives for the NCA site and for the ACh binding sites were determined by competitive inhibition of radioligand binding.

Binding to the ACh sites was examined by inhibition of [^{3}H]-ACh binding (Fig. 5). For each of the four compounds, the inhibition was somewhat better fit by a two-site model, rather than a single-site model, and this difference was most prominent for 3-AEB (Fig. 5B). The equilibrium dissociation constants (K_i values) calculated from the concentrations yielding 50% inhibition, as determined by nonlinear regression with a two-site model, are summarized in Table 1. The data suggest that EB and the azido derivatives differ in affinity for each of the two ACh binding sites, as does *d*-tubocurarine.

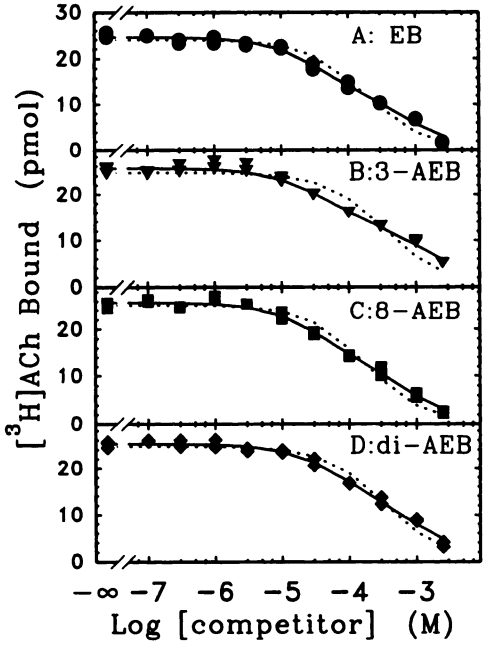

Fig. 5. Inhibition of [^{3}H]ACh binding by EB, 3-AEB, 8-AEB, and di-AEB. Low specific activity AChR-rich membranes (50 μg) were incubated with 150 nM [^{3}H]ACh and varying concetrations of EB (A), 3-AEB (B), 8-AEB (C), or di-AEB (D). After determination of bound [^{3}H]ACh, each set of data was fitted to models for inhibition at a single binding site (– – –) and at two equimolar binding sites (——), as described in Experimental Procedures. Nonspecific binding was determined by the inclusion of 1 mM carbamylcholine but was not subtracted from the data shown.

TABLE 1

Equilibrium inhibition constants for binding of EB and azido derivatives to the Ach binding sites and the NCA site

The equilibrium dissociation constants were calculated from the K_{app} values as described in Experimental Procedures. The respective K_{app} values were obtained from the data shown in Fig. 5–7. The K_d for [^{3}H]ACh was 20 nM and that for *d*-[^{3}H]tubocurarine was 50 nM, as determined independently (data not shown). The errors are the standard errors determined by the fitting routine.

Competitor	[^{3}H]ACh		*d*-[^{3}H]Tubocurarine	[^{3}H]PCP
	K_{i1}	K_{i2}		
			μM	
EB	5.2 ± 1	98 ± 50	4.0 ± 1	0.59 ± 0.06
3-AEB	6.2 ± 2	250 ± 300	7.1 ± 1	3.2 ± 0.3
8-AEB	5.0 ± 1	90 ± 50	1.9 ± 0.2	1.5 ± 0.2
Di-AEB	9.7 ± 2	160 ± 130	4.7 ± 0.8	1.1 ± 0.2

To determine whether the azide compounds bound preferentially to the ACh binding site with high affinity or low affinity for *d*-tubocurarine, the binding of *d*-[^{3}H]tubocurarine in the presence of varying concentrations of each compound was examined. A relatively low concentration of *d*-[^{3}H]tubocurarine (100 nM) was used to occupy predominantly the high affinity binding site. Inhibition of binding by EB and each of the azido compounds was well fit according to a single-site model (data not shown). Calculation of the K_i values for the compounds using the independently determined K_d for the high affinity binding of *d*-[^{3}H]tubocurarine and the K_{app} determined from the fit of the data yielded the values shown in Table 1. The affinities of the compounds for the high affinity site were similar, ranging from 2 to 7 μM. The individual K_i values compared well with the lower K_i values determined by inhibition of [^{3}H]ACh binding, with the largest difference being 2.5-fold for 8-AEB. Thus, EB and the azido derivatives bind with similar affinities to the ACh binding site with high affinity for *d*-tubocurarine.

Although each of the four compounds clearly binds to the ACh binding sites, EB is a potent NCA that binds the AChR with an equilibrium dissociation constant of 200 nM in the presence of an agonist, as measured by fluorescence (data not shown) (22). An objective of synthesizing the azido analogs was to determine the binding site locus for EB within the ion channel of the AChR. To determine whether the lack of labeling at the NCA site was due to loss of binding, each of the compounds was tested for inhibition of [^{3}H]PCP binding (Fig. 6; Table 1). All of the compounds specifically inhibited [^{3}H]-PCP binding in the presence of 100 μM carbamylcholine. The affinity of EB determined from [^{3}H]PCP inhibition was 590 nM (Fig. 6A). The affinities of the azide analogs were only slightly reduced, compared with that of EB; the values for di-AEB and 8-AEB were reduced about 2-fold, whereas the affinity of 3-AEB was reduced 5-fold (Table 1). These changes in affinity are insufficient to account for the lack of apparent labeling at the NCA site, because most labeling experiments used concentrations sufficient to yield substantial binding.

The binding experiment in Fig. 6 was performed in the presence of carbamylcholine to induce the desensitized conformation of the AChR, and the inhibition reflects the ability of the competitors to bind to this conformation. In the absence of carbamylcholine the AChR is predominantly in the resting conformation and competition for [^{3}H]PCP binding occurs at higher concentrations (>10-fold) (data not shown). Thus, the azide derivatives prefer the desensitized conformation for binding at the NCA site, as does EB. Because the presence of carbamylcholine reduced the yield of fluorescent adducts while enhancing the binding at the NCA site, the lack of labeling at

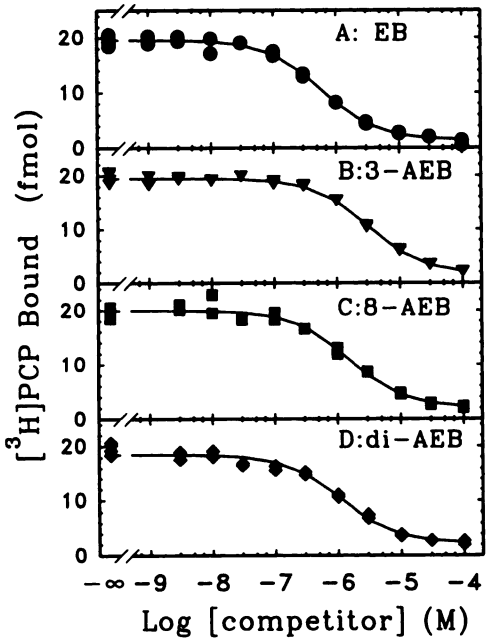

Fig. 6. Inhibition of [^{3}H]PCP binding by EB, 3-AEB, 8-AEB, and di-AEB. AChR-rich membranes (50 μg, 375 nM ACh binding sites, in a total volume of 200 μl of HTPS) were incubated with 0.4 nM [^{3}H]PCP, 100 μM carbamylcholine, and varying concentrations of EB (A), 3-AEB (B), 8-AEB (C), or di-AEB (D). After determination of bound [^{3}H]PCP, each set of data was fitted to the model for inhibition at a single binding site (——), as described in Experimental Procedures.

the NCA site must be attributable to a lack of reaction or to a nonfluorescent adduct.

Site specificity of photoaffinity labeling. The binding data and the pharmacological specificity of labeling of the α and γ subunits are consistent with labeling of the ACh binding site that has high affinity for *d*-tubocurarine, which is composed of the α/γ subunit combination. To demonstrate that specific labeling was correlated with binding, the relative amount of labeling was determined with increasing concentrations of 3-AEB (Fig. 7). Labeling was quantitated by two-dimensional densitometric scanning of photographic negatives of subunits separated by SDS-PAGE, as described in Experimental Procedures. As calculated from the difference between the total labeling and the nonspecific labeling, specific labeling of the α subunit and the γ subunit was saturated by 5 μM 3-AEB and could be fit to a single-binding site model, with K_{app} values of 1.2 and 1.1 μM, respectively (Fig. 7). The subunits were clearly labeled in parallel, but with K_{app} values lower than the K_i values of ~6 μM determined in [^{3}H]ACh and *d*-[^{3}H]tubocurarine binding assays. Specific labeling of neither the δ subunit nor the β subunit was observed, even at the highest concentrations of label used (50–100 μM) (data not shown). The nonlinear nonspecific reaction (in the presence of carbamylcholine) with the α subunit (Fig. 7A) could be due to low level labeling at the NCA site.

Inhibition of labeling by carbamylcholine (Fig. 8A) or by *d*-tubocurarine (Fig. 8B) occurred at concentrations consistent with binding to the ACh binding sites. Inhibition by carbamylcholine was well fit by a single-site model (Fig. 8A) for the both the α subunit and the γ subunit, with similar K_{app} values of 1.1 and 0.8 μM, respectively. Inhibition by *d*-tubocurarine of labeling of the γ subunit was also well fit by a single-binding site model, with a K_{app} of 0.2 μM, whereas inhibition by *d*-tubocurarine of labeling of the α subunit was better fit by a two-site model than a single-site model (Fig. 8B). The single-site fit for

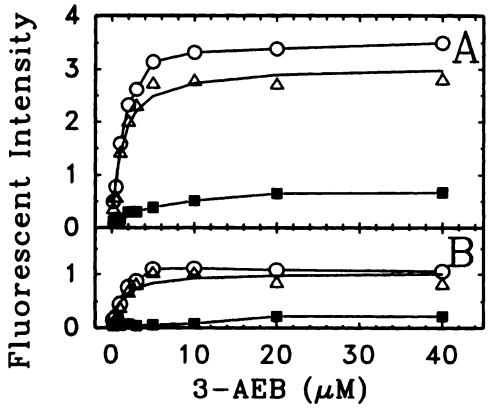

Fig. 7. Labeling of α and γ subunits and 3-AEB concentration dependence. AChR-rich membranes (50 μg, 1.4 nmol of ACh sites/mg) were equilibrated in the dark with the indicated concentrations of 3-AEB, in the absence or presence of 250 μM carbamylcholine, in 2 ml of HTPS. Samples were irradiated with visible light for 2 min and the AChR subunits were separated by SDS-PAGE. Relative fluorescence incorporation into the α (A) and γ (B) subunits was quantitated by densitometric scanning of a negative photograph of the gel, as described in Experimental Procedures. Specific labeling (Δ) was calculated from the difference in labeling in the absence (○) and in the presence (■) of carbamylcholine and was fitted to the model for a single binding site (——). The K_{app} values were 1.2 μM for labeling of the α subunit and 1.1 μM for labeling of the γ subunit. This experiment was performed three times with similar results.

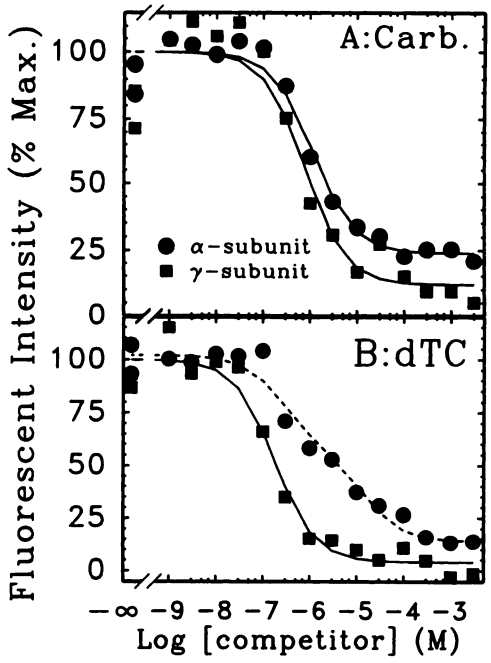

Fig. 8. Inhibition of 3-AEB labeling by *d*-tubocurarine and carbamylcholine. AChR-rich membranes (50 μg, 1.4 nmol of ACh sites/mg) were labeled with 5 μM 3-AEB in 1 ml of HTPS in the presence of the indicated concentrations of carbamylcholine (A) or *d*-tubocurarine (B). Samples were irradiated with visible light for 2 min and the AChR subunits were separated by SDS-PAGE. Relative fluorescence of the α subunits (●) and γ subunits (■) was quantitated by densitometric scanning of negative photographs of gel fluorescence, as described in Experimental Procedures. Each set of data was fitted by nonlinear regression to the model for inhibition at a single binding site (——), as described in Experimental Procedures, and is plotted as the percentage of the maximum determined from the nonlinear regression. For inhibition by *d*-tubocurarine of α subunit labeling, the data were also fit to a two-site model (– – –) (B); only the fit for the two-site model is shown. The K_{app} values for inhibition of labeling by carbamylcholine are 1.1 μM for the α subunit and 0.8 μM for the γ subunit. As determined by regression to the single-site model, the K_{app} values for inhibition of labeling by *d*-tubocurarine are 1.8 μM for the α subunit (not shown) and 0.2 μM for the γ subunit (——) (B). Regression to a two-site model for *d*-tubocurarine inhibition of α subunit labeling (– – –) (B) yielded K_{app} values of 0.3 and 14 μM. Each experiment was performed five times with similar results.

d-tubocurarine inhibition of α subunit labeling yielded a K_{app} of 1.8 μM (data not shown), compared with K_{app} values of 0.3 and 14 μM from the two-site fit. The lower K_{app} for the two-site fit corresponds well to the K_{app} determined for inhibition of γ subunit labeling and is consistent with inhibition at the binding site with high affinity for *d*-tubocurarine. The biphasic inhibition by *d*-tubocurarine of α subunit labeling demonstrates that 3-AEB labels both ACh binding sites. The inhibition by carbamylcholine is consistent with single-site inhibition, suggesting that labeling by 3-AEB does not discriminate strongly between the two sites.

Fluorescence of labeled AChR subunits. To approximate the extent of reaction of the AChR with 3-AEB, the fluorescence emission spectra of α and γ subunits were compared with those of EB and of 3-AEB that had been photolyzed. AChR were labeled with 3-AEB and the α and γ subunits were then isolated by preparative SDS-PAGE. Uncorrected spectra for the α and γ subunits are shown in Fig. 9A. Spectra were collected from subunits isolated from membranes labeled in the absence and presence of carbamylcholine to define nonspecific labeling. The spectra of the nonspecifically labeled α and γ

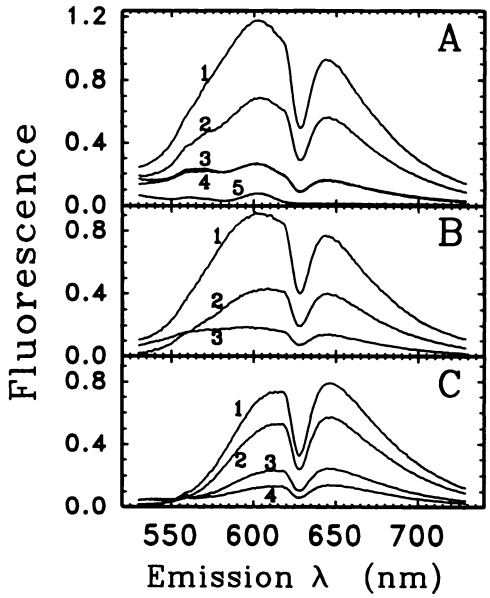

Fig. 9. Fluorescence emission spectra of 3-AEB-labeled α and γ subunits. AChR-rich membranes were labeled with 5 μM 3-AEB in the absence or presence of carbamylcholine, and the α and γ subunits were isolated as described in Experimental Procedures. For comparison, the spectra of EB and photoreacted 3-AEB were also collected. To generate photoreacted 3-AEB, three conditions were used; 3-AEB was diluted to 10 μM in water, in HTPS, or in 10 mM DTT, in the dark, and was then exposed to UV light for 30 sec. All samples were further diluted in 10 mM Tris, pH 6.8, 0.1% SDS, for collection of the spectra. The AChR subunits were diluted to 50 μg/ml. A, Uncorrected fluorescence emission spectra of the following: *spectrum 1*, α subunit labeled in the absence of carbamylcholine; *spectrum 2*, γ subunit labeled in the absence of carbamylcholine; *spectrum 3*, γ subunit labeled in the presence of carbamylcholine; *spectrum 4*, α subunit labeled in the presence of carbamylcholine; *spectrum 5*, buffer only. B, Fluorescence emission spectra of the α subunit (*spectrum 1*) and the γ subunit (*spectrum 2*) corrected for nonspecific labeling, obtained by subtracting A, *spectrum 4*, from A, *spectrum 1*, and A, *spectrum 3*, from A, *spectrum 2*, respectively. Nonspecific labeling of the α subunit (*spectrum 3*) was obtained by subtracting A, *spectrum 5*, from A, *spectrum 4*. C, Fluorescence emission spectra, corrected for buffer background, of the following: *spectrum 1*, 100 nM EB; *spectrum 2*, 100 nM 3-AEB photoreacted in 10 mM DTT; *spectrum 3*, 100 nM 3-AEB photoreacted in HTPS; *spectrum 4*, 100 nM 3-AEB photoreacted in water. The decrease in the spectra at 630 nm are a fluorometer artifact (see Experimental Procedures).

subunits were nearly identical (Fig. 9A, *spectra 3* and *4*). Subtraction of the buffer background contribution to the spectrum (Fig. 9A, *spectrum 5*) yielded the corrected nonspecific labeling (Fig. 9B, *spectrum 3*) shown for the α subunit only. Subtraction of the corresponding nonspecifically labeled subunit spectra from the spectra of the subunits labeled in the absence of carbamylcholine yielded spectra of the specific component of labeling (Fig. 9B, *spectra 1* and *2*). The spectra revealed peaks at 600 nm for the specific component. The intensity of the α subunit signal was approximately twice that of the γ subunit and about 5 times that of the nonspecific component. The peaks were sharper for the specific components, compared with the broader, flat, emission spectrum of the nonspecific labeling.

The intensity of the specific labeling was compared with the emission spectra of 100 nM EB (Fig. 9C, *spectrum 1*) and of 100 nM 3-AEB that had been reacted with DTT (Fig. 9C, *spectrum 2*), photolyzed in HTPS (Fig. 9C, *spectrum 3*), or photolyzed in water (Fig. 9C, *spectrum 4*). The spectra of the subunits were collected at a concentration of 50 μg/ml, which corresponds to ~1 μM subunit and yielded fluorescence intensity comparable to that of 100 nM EB (Fig. 9, B, *spectrum 1*, versus C, *spectrum 1*). This suggested substantial specific reaction of 3-AEB at the ACh site, with approximately 10% of the subunits. This estimate assumes similar fluorescence yields from the adducts and from EB. This is likely to be an incorrect assumption. However, photolyzed 3-AEB and 3-AEB reacted with DTT had lower fluorescence intensities than did the same concentration of EB (Fig. 9C). Thus, it seems likely that the adducts resulting from specific reaction at the ACh binding site would be less fluorescent than EB. These results suggest that the reaction at the ACh binding site is quite efficient.

Discussion

The three azido derivatives of EB, i.e., 3-AEB, 8-AEB, and di-AEB, were synthesized and shown to act as photoaffinity ligands at the ACh binding sites of the AChR. Inhibition of 3-AEB labeling by *d*-tubocurarine indicated reaction at the α subunits of both ACh sites. Photoaffinity labeling occurs at both the α subunit and the apposing γ subunit at the site with high affinity for *d*-tubocurarine, whereas labeling occurs only at the α subunit of the second site, composed of α and δ subunits. 3-AEB reactivity with the non-α subunit of each site is, therefore, sensitive to the local environment of the site. It is likely that the difference in reactivity reflects the specificity of the sites for ligands such as *d*-tubocurarine. The fluorescence spectra of isolated α subunits and γ subunits suggest efficient labeling, with a stoichiometry near 10%.

The pattern of photoaffinity labeling was consistent with reaction at the ACh binding sites. However, the binding of EB to the NCA site was known to be allosterically regulated by ligands that bind the ACh binding site (22). To demonstrate that the inhibition of photoaffinity labeling was not due to allosterically induced conformational changes but reflected competitive inhibition, three distinct competitive ligands for the ACh binding site, i.e., carbamylcholine, *d*-tubocurarine, and α-bungarotoxin, were shown to block photoaffinity labeling (Fig. 3). The affinities of EB and its azido derivatives for the NCA site were allosterically enhanced by carbamylcholine and decreased by α-bungarotoxin, as observed by competitive inhibition of [^{3}H]PCP binding (22).[1] Photoaffinity labeling was not prevented by NCAs that bind either the desensitized conformation (PCP and meproadifen) or the resting conformation (tetracaine) (32). These observations demonstrate that inhibition of photoaffinity labeling at the ACh binding sites is competitive and not due to allosteric effects.

Inhibition of [^{3}H]ACh and *d*-[^{3}H]tubocurarine binding by EB and its azido derivatives showed that these ligands bind to the ACh binding site that has high affinity for *d*-tubocurarine with an affinity of 2–10 μM. [^{3}H]ACh binding data were better fit by a two-site model than a single-site model (Fig. 5), suggesting selectivity for one of the binding sites. *d*-[^{3}H]Tubocurarine binding data yielded dissociation constants consistent with the lower of the two dissociation constants determined from inhibition of [^{3}H]ACh binding (Table 1). Thus, EB and the azido derivatives display a site selectivity qualitatively similar to that of *d*-tubocurarine but with a lower degree of selectivity.

Labeling of the α and γ subunits by 3-AEB was concentration

[1] D. Jackson and S. E. Pedersen, unpublished observations.

dependent and displayed similar K_{app} values of ~1 μM for each subunit (Fig. 7). These K_{app} values are 5-fold lower than the K_i measured for binding to the high affinity *d*-tubocurarine binding site. This discrepancy may reflect the details of the photoaffinity reaction or differences in the conditions used for the binding assays and the photoaffinity reaction. It is possible that the photoactivated aryl nitrene has higher affinity than the parent azide or that the activated state has a long lifetime that would permit full labeling at subsaturating concentrations. The latter possibility is unlikely, because labeling was not strongly affected by scavenging reagents such as 2-mercaptoethanol or oxidized glutathione (data not shown). The irradiation time yielded maximum labeling and longer irradiation produced no further increase in specific or nonspecific labeling, suggesting complete photolysis of the azide within this time.

The labeling of the γ subunit was consistent with binding to and reaction at the ACh site with high affinity for *d*-tubocurarine (15). In contrast, there was no evidence of specific reaction with the δ subunit, even at concentrations of up to 100 μM 3-AEB (or the other azide derivatives). Although this might have been due to lack of binding to the site with lower affinity for *d*-tubocurarine, as suggested by the biphasic inhibition of [^{3}H]ACh binding (Fig. 5; Table 1), it is more likely due to lack of reactivity towards the δ subunit. Inhibition of photoaffinity labeling of the α and γ subunits by carbamylcholine displayed similar K_{app} values (~1 μM) for the two subunits and the data were fit reasonably well by a single-site model for inhibition (Fig. 8). In contrast, inhibition of labeling by *d*-tubocurarine differed for the two subunits, with labeling of the γ subunit being inhibited at low concentrations (~0.3 μM) and well fit by a single-site model, whereas inhibition of labeling of the α subunit was better fit by a two-site model for inhibition. These data suggest that the α subunit is labeled via both ACh binding sites, whereas the γ subunit is labeled only via the site with high affinity for *d*-tubocurarine. The lower K_{app} for inhibition of α subunit labeling corresponded to that obtained for the γ subunit.

It appears, therefore, that lack of labeling of the δ subunit reflects not lack of binding at this ACh binding site but, rather, intrinsic differences in reactivity at the two binding sites. This suggests that the amino acids that react with 3-AEB may be unique to the γ subunit and thus contribute to the site specificity. This will be addressed through additional experiments to identify the labeled amino acid(s) in the γ subunit. The apparently high level of labeling makes this a feasible project, even without a radioactive label.

The difference in labeling of the γ subunit by the three azido compounds may reflect the details of the proximity of the azide to the labeled amino acid(s). The overall labeling pattern is similar for the three derivatives, except for the reaction at the γ subunit, where 3-AEB clearly reacts better than 8-AEB or di-AEB. Differences in labeling of the α subunit are less striking; 3-AEB and 8-AEB yielded comparable levels of reaction and di-AEB labeling was somewhat weaker. If the labeled residue in the γ subunit is near the 3-position of EB, rather than the 8-position, then 3-AEB would be predicted to react more efficiently, as observed. However, this would not simply account for the poorer reactivity of di-AEB, which has both azide moieties. The poorer reaction of di-AEB may reflect its shorter half-life or preferential reactivity of its 8-azido moiety, compared with the 3-azido moiety.

EB has been characterized as a NCA that binds at the ion channel of the AChR with high affinity (22, 30). One goal of synthesizing photoaffinity derivatives of EB was to identify this site, to correlate the results of fluorescence experiments and fluorescence energy transfer experiments (33, 34) with the exact binding locus. Thus, the lack of photoaffinity labeling at the NCA site was somewhat disconcerting and could not be explained by changes in binding affinity due to changing the 3- or 8-amines to azides. The lack of reaction could be due to the formation of nonfluorescent adducts that were not observed. More likely is poorer reaction due to interaction with less reactive aliphatic residues (35) in the second hydrophobic sequence, M2, thought to constitute the NCA site. The experiments shown here do not distinguish these possibilities. A small amount of reaction with 3-AEB or with di-AEB at the α subunit in the presence of carbamylcholine could be blocked by addition of PCP (Fig. 4). Thus, the apparently efficient reaction at the ACh sites may eclipse weaker labeling at the NCA site. Radiolabeled ligands would be helpful in distinguishing these possibilities but are not yet available. Because the photoaffinity labeling reaction can be induced by visible irradiation, it is unlikely that specific activation of amino acids within the ACh binding sites can account for the better labeling.

In the mouse AChR, site-directed mutagenesis has identified three residues of the γ and δ subunits that appear to account for the site selectivity of trimethyl-*d*-tubocurarine (18). It will be of interest to determine whether the homologous residues confer site selectivity in the *Torpedo* AChR and whether such residues are also important for agonist site selectivity. Although these residues appear to solely account for the site selectivity of trimethyl-*d*-tubocurarine binding to the mouse AChR, they are clearly not the only residues on the γ and δ subunits to affect ligand binding. In addition to the conserved γTrp-56 and δTrp-57 identified by *d*-[^{3}H]tubocurarine labeling of *Torpedo* AChR (17), Czajkowski *et al.* (36) recently identified Asp-180 of the δ subunit as likely being in the vicinity of the ACh binding site. This residue is conserved in the γ subunit and also would not be predicted to account for site selectivity.

Acknowledgments

David Jackson and Karen Hong are thanked for technical assistance. David Chiara and Jonathan B. Cohen are thanked for their contribution of *d*-[^{3}H]-tubocurarine.

References

1. Raftery, M. A., M. W. Hunkapiller, C. D. Strader, and L. E. Hood. Acetylcholine receptor: complex of homologous subunits. *Science (Washington D. C.)* **208**:1454–1457 (1980).
2. Noda, M., H. Takahashi, T. Tanabe, M. Toyosato, S. Kikyotani, Y. Furutani, T. Hirose, H. Takashima, S. Inayama, T. Miyata, and S. Numa. Structural homology of *Torpedo californica* acetylcholine receptor subunits. *Nature (Lond.)* **302**:528–532 (1983).
3. Unwin, N. Nicotinic acetylcholine receptor at 9 Å resolution. *J. Mol. Biol.* **229**:1101–1124 (1993).
4. Devillers-Thiery, A., J. L. Galzi, J. L. Eisele, S. Bertrand, and J.-P. Changeux. Functional architecture of the nicotinic acetylcholine receptor: a prototype of ligand-gated ion channels. *J. Membr. Biol.* **136**:97–112 (1993).
5. Damle, V. N., and A. Karlin. Affinity labeling of one or two α-neurotoxin binding sites in acetylcholine receptor from *Torpedo californica*. *Biochemistry* **17**:2039–2045 (1978).
6. Wolosin, J., A. Lyddiatt, J. O. Dolly, and E. A. Barnard. Stoichiometry of the ligand-binding sites in the acetylcholine-receptor oligomer from muscle and electric organ. *Eur. J. Biochem.* **109**:495–505 (1980).
7. Wilson, P. T., J. M. Gershoni, E. Hawrot, and T. L. Lentz. Binding of α-bungarotoxin to proteolytic fragments of the α subunit of *Torpedo* acetylcholine receptor analyzed by protein transfer on positively charged membrane filters. *Proc. Natl. Acad. Sci. USA* **81**:2553–2557 (1984).
8. Kao, P. N., A. J. Dwork, R. J. Kaldany, M. L. Silver, J. Widemann, S. Stein, and A. Karlin. Identification of the α subunit half-cystine specifically labeled

by an affinity reagent for the acetylcholine receptor binding site. *J. Biol. Chem.* **259**:11662–11665 (1984).
9. Abramson, S. N., Y. Li, P. Culver, and P. Taylor. An analog of lophotoxin reacts covalently with Tyr^{190} in the α-subunit of the nicotinic acetylcholine receptor. *J. Biol. Chem.* **264**:12666–12672 (1989).
10. Dennis, M., J. Giraudat, F. Kotzyba-Hibert, M. Goeldner, C. Hirth, J.-Y. Chang, C. Lazure, M. Chretien, and J.-P. Changeux. Amino acids of the *Torpedo marmorata* acetylcholine receptor α subunit labeled by a photoaffinity ligand for the acetylcholine binding site. *Biochemistry* **27**:2346–2357 (1988).
11. Middleton, R. E., and J. B. Cohen. Mapping of the acetylcholine binding site of the nicotinic acetylcholine receptor: [^{3}H]nicotine as an agonist photoaffinity label. *Biochemistry* **30**:6987–6997 (1991).
12. Cohen, J. B., S. D. Sharp, and W. S. Liu. Structure of the agonist-binding site of the nicotinic acetylcholine receptor: [^{3}H]acetylcholine mustard identifies residues in the cation-binding subsite. *J. Biol. Chem.* **266**:23354–23364 (1991).
13. Chaturvedi, V., D. L. Donnelly-Roberts, and T. L. Lentz. Effects of mutations of *Torpedo* acetylcholine receptor α1 subunit residues 184–200 on α-bungarotoxin binding in a recombinant fusion protein. *Biochemistry* **32**:9570–9576 (1993).
14. Neubig, R. R., and J. B. Cohen. Equilibrium binding of [^{3}H]tubocurarine and [^{3}H]acetylcholine by *Torpedo* postsynaptic membranes: stoichiometry and ligand interactions. *Biochemistry* **18**:5464–5475 (1979).
15. Pedersen, S. E., and J. B. Cohen. *d*-Tubocurarine binding sites are located at α-γ and α-δ subunit interfaces of the nicotinic acetylcholine receptor. *Proc. Natl. Acad. Sci. USA* **87**:2785–2789 (1990).
16. Blount, P., and J. P. Merlie. Molecular basis of the two nonequivalent ligand binding sites of the muscle nicotinic acetylcholine receptor. *Neuron* **3**:349–357 (1989).
17. Chiara, D. C., and J. B. Cohen. Identification of amino acids contributing to high and low affinity *d*-tubocurarine (dTC) sites on the *Torpedo* nicotinic acetylcholine receptor. *Biophys. J.* **62**:A106 (1992).
18. Sine, S. M. Molecular dissection of subunit interfaces in the acetylcholine receptor: identification of residues that determine curare selectivity. *Proc. Natl. Acad. Sci. USA* **90**:9436–9440 (1993).
19. Schimerlick, M. I., U. Quast, and M. A. Raftery. Ligand-induced changes in membrane-bound acetylcholine receptor observed by ethidium fluorescence. 1. Equilibrium studies. *Biochemistry* **18**:1884–1890 (1979).
20. Schimerlick, M. I., U. Quast, and M. A. Raftery. Ligand-induced changes in membrane-bound acetylcholine receptor observed by ethidium fluorescence. 3. Stopped-flow studies with histrionicotoxin. *Biochemistry* **18**:1902–1906 (1979).
21. Quast, U., M. I. Schimerlick, and M. A. Raftery. Ligand-induced changes in membrane-bound acetylcholine receptor observed by ethidium fluorescence. 2. Stopped-flow studies with agonists and antagonists. *Biochemistry* **18**:1891–1901 (1979).
22. Herz, J. M., D. A. Johnson, and P. Taylor. Interaction of noncompetitive inhibitors with the acetylcholine receptor: the site specificity and spectroscopic properties of ethidium binding. *J. Biol. Chem.* **262**:7238–7247 (1987).
23. Firth, W. J., C. L. Watkins, D. E. Graves, and L. W. Yielding. Synthesis and characterization of ethidium analogs: emphasis on amino and azido substituents. *J. Heterocyclic Chem.* **20**:759–765 (1983).
24. Garland, F., D. E. Graves, L. W. Yielding, and H. C. Cheung. Comparative studies of the binding of ethidium bromide and its photoreactive analogues to nucleic acids by fluorescence and rapid kinetics. *Biochemistry* **19**:3221–3226 (1980).
25. Pedersen, S. E., E. B. Dreyer, and J. B. Cohen. Location of ligand-binding sites on the nicotinic acetylcholine receptor α-subunit. *J. Biol. Chem.* **261**:13735–13743 (1986).
26. Krodel, E. K., R. A. Beckman, and J. B. Cohen. Identification of a local anesthetic binding site in nicotinic post-synaptic membranes isolated from *Torpedo marmorata* electric tissue. *Mol. Pharmacol.* **15**:294–312 (1979).
27. Laemmli, U. K. Cleavage of structural proteins during the assembly of the head of bacteriophage T4. *Nature (Lond.)* **227**:680–685 (1970).
28. Hager, D. A., and R. R. Burgess. Elution of proteins from sodium dodecyl sulfate-polyacrylamide gels, removal of sodium dodecyl sulfate, and renaturation of enzymatic activity: results with *sigma* subunit of *Escherichia coli* RNA polymerase, wheat germ DNA topoisomerase and other enzymes. *Anal. Biochem.* **109**:76–86 (1980).
29. Pedersen, S. E., P. C. Bridgman, S. D. Sharp, and J. B. Cohen. Identification of a cytoplasmic region of the *Torpedo* nicotinic acetylcholine receptor α-subunit by epitope mapping. *J. Biol. Chem.* **265**:569–581 (1990).
30. Herz, J. M., S. J. Kolb, T. Erlinger, and E. Schmid. Channel permeant cations compete selectively with noncompetitive inhibitors of the nicotinic acetylcholine receptor. *J. Biol. Chem.* **266**:16691–16698 (1991).
31. Herz, J. M., and S. J. Atherton. Steric factors limit access to the noncompetitive inhibitor site of the nicotinic acetylcholine receptor. *Biophys. J.* **62**:74–76 (1992).
32. Cohen, J. B., and N. P. Strnad. Permeability control and desensitization by nicotinic acetylcholine receptors, in *Molecular Mechanisms of Desensitization to Signal Molecules* (T. M. Konijn, ed.). Springer Verlag, Berlin, 257–273 (1987).
33. Herz, J. M., D. A. Johnson, and P. Taylor. Distance between the agonist and noncompetitive inhibitor sites on the nicotinic acetylcholine receptor. *J. Biol. Chem.* **264**:12439–12448 (1989).
34. Arias, H. R., C. F. Valenzuela, and D. A. Johnson. Quinacrine and ethidium bind to different loci on the *Torpedo* acetylcholine receptor. *Biochemistry* **32**:6237–6242 (1993).
35. Bayley, H., and J. R. Knowles. Photogenerated reagents for membrane labeling. 1. Phenylnitrene formed within the lipid bilayer. *Biochemistry* **17**:2414–2419 (1978).
36. Czajkowski, C., C. Kaufmann, and A. Karlin. Negatively charged amino acid residues in the nicotinic receptor δ subunit that contribute to the binding of acetylcholine. *Proc. Natl. Acad. Sci. USA* **90**:6285–6289 (1993).

Send reprint requests to: Steen E. Pedersen, Department of Molecular Physiology and Biophysics, Baylor College of Medicine, One Baylor Plaza, Houston, TX 77030.